Commun. Theor. Phys. **74** (2022) 105601 (14pp) https://doi.org/10.1088/1572-9494/ac8fe2

Dynamics of cooperative transport by multiple kinesin motors and diffusing microtubule-associated proteins

Yao Wang[1,2], **Yu-Ru Liu**[1,2], **Peng-Ye Wang**[1,2] and **Ping Xie**[1,2,*]

[1] Key Laboratory of Soft Matter Physics, Institute of Physics, Chinese Academy of Sciences, Beijing 100190, China
[2] School of Physical Sciences, University of Chinese Academy of Sciences, Beijing 100049, China

E-mail: pxie@aphy.iphy.ac.cn

Received 22 July 2022, revised 6 September 2022
Accepted for publication 7 September 2022
Published 30 September 2022

Abstract

In eukaryote cells, cargos are often transported cooperatively by kinesin motors and nonmotor microtubule-associated proteins (MAPs). The prior *in vitro* experimental data showed that the velocity of the cargo transported by kinesin motors and Ndc80 (a member of MAP) proteins of truncated coiled-coil stalks decreases sensitively with the increase of the ratio of Ndc80 to motor number. However, the underlying mechanism of Ndc80 affecting sensitively the cooperative cargo transport by kinesin motors is unclear. To understand the mechanism, here we study numerically the cooperative cargo transport by kinesin motors and Ndc80 proteins. Our results showed that for the case of the motors and Ndc80 proteins with truncated short stalks, as used in the experiments, the calculated results reproduce quantitatively the prior experimental data. The mechanism of the cargo velocity decreasing sensitively with the ratio of Ndc80 to motor number is revealed. By contrast, for the case of the motors and Ndc80 proteins with full-length long stalks, the velocity of the cargo decreases slowly with the increase in the ratio of Ndc80 to kinesin number. Our results thus give an explanation of why the kinesin motors working in the cell have long stalks.

Supplementary material for this article is available online

Keywords: intracellular transport, molecular motor, kinesin, microtubule-associated protein, Ndc80

(Some figures may appear in colour only in the online journal)

1. Introduction

Efficient cargo transports in cells are performed by motor proteins such as kinesin motors [1–6]. Nonmotor microtubule-associated proteins (MAPs) are also involved in intracellular transports [6–14]. Kinesin motors can move directionally along microtubule (MT) filaments towards the plus end by the hydrolysis of ATP [3–5]. Many MAPs without ATPase activity can diffuse unbiasedly along the MT filaments [13–15]. Ndc80 protein is a member of diffusing MAPs [16, 17]. It is the key MT-binding component of the kinetochore, participating in the transport of kinetochores [17–21]. During prometaphase in cell division, Ndc80 proteins cooperate with kinesin-7 CENP-E motors to transport the kinetochore towards the MT plus end [22–24]. Recently, Chakraborty *et al* [17] studied in detail the cooperative cargo transport by multiple CENP-E motors and Ndc80 proteins, determining quantitatively the effect of the Ndc80 proteins on the dynamics of the cargo transport. For comparison, they also made studies with CENP-E motors being replaced by kinesin-1 motors [17]. Puzzlingly, they found experimentally that the presence of Ndc80 proteins has a sensitive effect on the reduction of the velocity of the cargo transport by multiple kinesin motors [17]. For example, in the case of kinesin-1

* Author to whom any correspondence should be addressed.

motors, the velocity decreases linearly with the increase of the ratio of the number of Ndc80 proteins to motors, and at the ratio of 0.8, the velocity decreases by about 2.7-fold relative to that in the absence of the Ndc80 [17]. For the case of CENP-E motors, as the ratio increases the velocity decreases much quicker and at the ratio of only 1, the velocity becomes nearly 0 [17]. By contrast, the experimental data showed that the velocity of the cooperative transports by multiple kinesin-1 motors is kept nearly unchanged with the motor number [25] and the velocity of the cooperative transports by multiple CENP-E motors at high motor concentrations decreases by about 1.4-fold relative to the velocity of the single motor [26].

While the dynamics of the cooperative cargo transport by multiple molecular motors have been studied intensively and extensively [27–41], the theoretical and numerical study of the dynamics of the cooperative cargo transport by multiple molecular motors and diffusing MAPs has not been paid much attention to. The underlying mechanism of the effect of the diffusing MAPs on the cooperative cargo transport by kinesin motors is unclear. In particular, the puzzling experimental results showing that the presence of Ndc80 proteins has a sensitive effect on the reduction of the cargo velocity have not been explained up to now [17]. In addition, the difference in the feature for the motor-number dependence of the velocity of the cooperative transports by multiple kinesin-1 motors from that by multiple CENP-E motors [25, 26] has not been explained.

To understand the above-mentioned mechanism and to explain the puzzling experimental data, in this work we analyze the cooperative cargo transport by multiple kinesin motors and Ndc80 proteins. As done in the experiments of Chakraborty *et al* [17], we also consider two families of kinesin motors—kinesin-1 and kinesin-7 CENP-E. Since the two heads of the motor are connected to the common coiled-coil stalk via the flexible neck linkers (NLs), it is argued that the relatively rigid stalk should rotate freely in a large range of the angle relative to the heads. Thus, we first use all-atom molecular dynamics (MD) simulations to validate the argument. The large free rotation of the stalk indicates that in the cooperative cargo transport by multiple motors a motor can move freely in a range of the distance on MT without experiencing any external force that arises from the stretching of its stalk, as argued before [30–36]. With the consideration of the presence of such a range, we show that the velocity of the cargo cooperatively transported by multiple kinesin motors versus the motor number can reproduce well the available experimental data. On the basis of the above studies, we then study the cooperative cargo transport by multiple kinesin motors and Ndc80 proteins with truncated stalks, as done in the experiments of Chakraborty *et al* [17], explaining quantitatively the experimental data. Furthermore, we study the cooperative cargo transport by multiple kinesin motors and Ndc80 proteins with full-length stalks, showing that the cargo velocity decreases only slowly with the ratio of Ndc80 to motor number.

2. Models for dynamics of single kinesin motors and dynamics of single Ndc80 proteins

2.1. Kinesin motor

Consider an external force, F, on the stalk of the motor, with F resisting the forward movement of the motor being defined to have a positive value. As it is known, during the processive stepping of the motor each step consists of a long dwell period, during which the position of the motor is kept unchanged, and a very short moving period, during which the position of the motor varies. In the single-molecule optical trapping experiments, the motor experiences a constant external force F during the dwell period. During the moving period, here we consider two models for the external force experienced by the motor to determine the stepping rate.

The first model is that during the moving period of one step the motor experiences the constant external force F that is equal to that during the dwell period before the occurrence of the moving period, as generally studied in the literature [27, 28, 34–41]. For the convenience of writing, this model is called the constant-force model here. Based on the model, the forward and backward stepping of the motor as the function of F can be written as [42–44]

$$k_{\rm F}^{(\rm M)} = \frac{\exp\left[\beta(E_0 - Fd^{(+)})\right]}{\exp\left[\beta(E_0 - Fd^{(+)})\right] + 1} k^{(+)}, \tag{1}$$

$$k_{\rm B}^{(\rm M)} = \frac{1}{\exp\left[\beta(E_0 - Fd^{(+)})\right] + 1} k^{(-)}, \tag{2}$$

where $k^{(+)}$ is the ATPase rate of the trailing head, $k^{(-)}$ is the ATPase rate of the leading head, E_0 is the internal energy of the motor gained from the consumption of an ATP to facilitate its forward movement, with E_0 being equal to the free energy change associated with the large conformational change and NL docking of the kinesin head induced by ATP binding, $d^{(+)}$ is the characteristic distance, and $\beta^{-1} = k_{\rm B}T$ is the Boltzmann constant times the absolute temperature. The velocity of the motor has the form

$$v_0 = (k_{\rm F}^{(\rm M)} - k_{\rm B}^{(\rm M)})d, \tag{3}$$

where $d = 8.2$ nm is the step size[45, 46].

The second model is that during the moving period of one step the motor experiences the varying external force, as studied recently [32, 47]. This is because even in the single molecule optical trapping experiments with the feedback to ensure a 'constant' load on the motor the moving time in one step is much shorter than the response time of the feedback, as discussed before [47–51]. For the cooperative cargo transport by multiple motors and MAPs, during the moving period of one motor in one step the other motors and MAPs are unmoved and thus the moving motor would experience a varying force arising from the stretching of the linkers connecting the common cargo and motors and MAPs. This model is called the varying-force model here. Based on the model, the forward and backward stepping rates can be written as [47]

$$k_{\rm F}^{(\rm M)} = \frac{\exp\left\{\beta[E_0 + \lambda(\varepsilon_0 - \varepsilon_1)]\right\}}{\exp\left\{\beta[E_0 + \lambda(\varepsilon_0 - \varepsilon_1)]\right\} + 1} k^{(+)}, \tag{4}$$

$$k_{\rm B}^{(\rm M)} = \frac{1}{\exp\{\beta[E_0 + \lambda(\varepsilon_{-1} - \varepsilon_0)]\} + 1} k^{(-)}, \quad (5)$$

where ε_0 is the potential energy of the motor in the position before taking the forward step, i.e. the potential energy during the dwell period, ε_1 the potential energy after the motor taking the forward step, ε_{-1} is the potential energy after the motor takes the backward step, and λ ($\leqslant 1$) is the splitting factor for the potential energy change between the forward stepping and no stepping, namely the futile chemomechanical coupling, or between the backward stepping and no stepping. The velocity of the motor can still be described by equation (3).

For the case of the single molecule optical trapping experiments, we denote by c_1 the effective spring coefficient of the optical trapping and the stalk of the motor. The potential energy ε_0 has the form $\varepsilon_0 = c_1(\Delta x)^2/2$, where Δx is the change in the position of the motor relative to that when the trapped bead is in its equilibrium position (with no trapping force on the bead) and the motor stalk is not stretched. Correspondingly, the external force on the motor is $F = c_1\Delta x$. After the motor taking a forward step of size d, the elastic potential energy becomes $\varepsilon_1 = c_1(\Delta x + d)^2/2$. After the motor taking a backward step of size d, the elastic potential energy becomes $\varepsilon_{-1} = c_1(\Delta x - d)^2/2$. By substituting the above expressions for ε_0, ε_1 and ε_{-1} into equations (4) and (5) we have

$$k_{\rm F}^{(\rm M)} = \frac{\exp\left\{\beta\left[E_0 - \lambda\left(Fd + c_1\frac{d^2}{2}\right)\right]\right\}}{\exp\left\{\beta\left[E_0 - \lambda\left(Fd + c_1\frac{d^2}{2}\right)\right]\right\} + 1} k^{(+)}, \quad (6)$$

$$k_{\rm B}^{(\rm M)} = \frac{1}{\exp\left\{\beta\left[E_0 - \lambda\left(Fd - c_1\frac{d^2}{2}\right)\right]\right\} + 1} k^{(-)}, \quad (7)$$

where it is noted that F is the external force on the motor during the dwell period before making the stepping.

The available single-molecule optical trapping experimental data indicated that the effective spring coefficient, c_1, of the optical trapping and the stalk of the kinesin motor is about 0.05 pN nm^{-1} [49] (noting that as the spring coefficient of the motor stalk has a value of about 0.3 pN nm^{-1} [52], it is approximately considered that c_1 is determined by the spring coefficient of the optical trapping). Thus, we take $c_1 =$ 0.05 pN nm^{-1} to fit the available single-molecule optical trapping experimental data to equations (3), (6) and (7). The biochemical data indicated that the ATPase rate of the leading head, $k^{(-)}$, is much smaller than that of the trailing head, $k^{(+)}$ [53], as discussed before [54, 55]. Thus, for a good approximation, we take $k^{(-)} = 0$ in this work. First, we focus on kinesin-1. For the varying-force model, by fitting the single-molecule data of Nishiyama *et al* [49] to equations (3), (6) and (7) (thick black line in figure 1(a)) we have $k^{(+)} =$ 130 s^{-1}, $E_0 = 2.1k_{\rm B}T$ and $\lambda = 0.4$ (table 1). For the constant-force model, with equations (1)–(3) the single-molecule data of Nishiyama *et al* [49] can also be reproduced well (thin green line in figure 1(a)) by taking $k^{(+)} = 130$ s^{-1}, $E_0 = 2.1k_{\rm B}T - \lambda c_1 d^2/2 = 1.94k_{\rm B}T$ and $d^{(+)} = \lambda d = 3.28$ nm (table 1), as studied before [47]. Second, we focus on

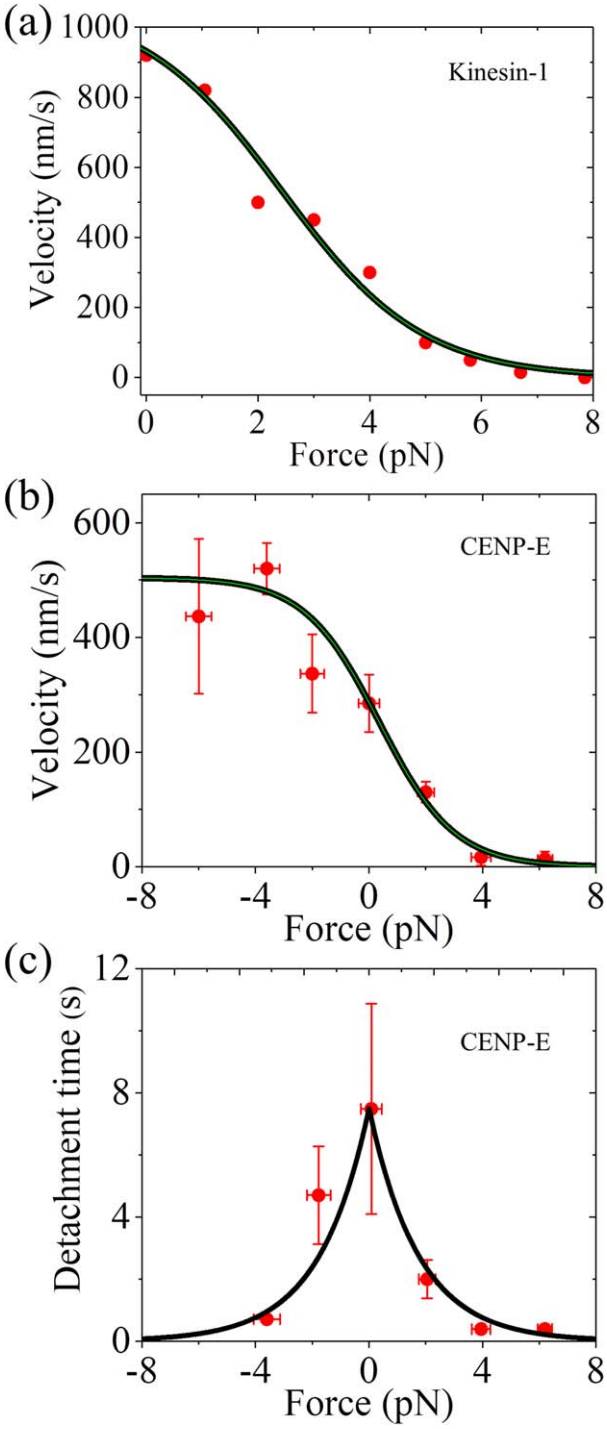

Figure 1. Dynamics of the single kinesin motors in the optical trapping experiments. (a) Velocity versus external force for kinesin-1. The thick black line represents theoretical results obtained with the varying-force model. The thin green line represents theoretical results obtained with the constant-force model. Circles are experimental data at saturating ATP (1 mM) measured by Nishiyama *et al* [49]. (b) Velocity versus external force for kinesin-7 CENP-E. The thick black line represents theoretical results obtained with the varying-force model. The thin green line represents theoretical results obtained with the constant-force model. Circles are experimental data for truncated CENP-E at saturating ATP (2 mM) measured by Gudimchuk *et al* [46]. (c) Detachment time versus external force for kinesin-7 CENP-E. The line represents theoretical results. Circles are experimental data for truncated CENP-E at saturating ATP (2 mM) measured by Gudimchuk *et al* [46].

Table 1. Parameter values for kinesin motors.

Parameters	Kinesin-1 Varying-force model	Kinesin-1 Constant-force model	CENP-E Varying-force model	CENP-E Constant-force model
$k^{(+)}$ (s^{-1})	130	130	61.5	61.5
E_D (k_BT)	2.1	1.94	0.43	0.28
λ	0.4	—	0.38	—
$d^{(+)}$ (nm)	—	3.28	—	3.11
$k_{off}^{(0)}$ (s^{-1})	1	1	1/7.5	1/7.5
F_{d1} (pN)	3	3	1.75	1.75
F_{d2} (pN)	1	1	1.75	1.75
μ (s^{-1})	5	5	0.4	0.4

Symbol '–' represents that the corresponding parameter value is not required in the model.

kinesin-7 CENP-E. For the varying-force model, by fitting the single-molecule data of Gudimchuk *et al* [46] for truncated CENP-E to equations (3), (6) and (7) (thick black line in figure 1(b)) we have $k^{(+)} = 61.5\ s^{-1}$, $E_0 = 0.43k_BT$ and $\lambda = 0.38$ (table 1). For the constant-force model, with equations. (1)–(3) the single-molecule data of Gudimchuk *et al* [46] can also be reproduced well (thin green line in figure 1(b)) by taking $k^{(+)} = 61.5\ s^{-1}$, $E_0 = 0.43k_BT - \lambda c_1 d^2/2 = 0.28k_BT$ and $d^{(+)} = \lambda d = 3.11$ nm (table 1).

Then, we determine the detachment of the kinesin motor. As done in the literature [28, 34, 38], for simplicity, we take the detachment rate of the motor versus the external force having the single-exponential form

$$k_{off} = k_{off}^{(0)} \exp\left(\frac{|F|}{F_{d1}}\right), \text{ when } F \geqslant 0, \tag{8}$$

$$k_{off} = k_{off}^{(0)} \exp\left(\frac{|F|}{F_{d2}}\right), \text{ when } F < 0, \tag{9}$$

where $k_{off}^{(0)}$ is the detachment rate under no external force, F_{d1} is the detachment force under the resisting force and F_{d2} is the detachment force under the assisting force. For kinesin-1, values of $k_{off}^{(0)}$, F_{d1} and F_{d2} are taken as follows. As usually done in the literature [34, 35, 38], we take $k_{off}^{(0)} = 1\ s^{-1}$ and $F_{d1} = 3$ pN (table 1). Since the available experimental data indicated that with the increase in the magnitude of the assisting load the run length of the kinesin-1 motor decreases much quicker than with the increase in the magnitude of the resisting load [45], implying that F_{d2} is smaller than F_{d1}. Thus, we take $F_{d2} = 1$ pN (table 1), which is inferred from the previous studies [28, 39]. For the truncated CENP-E, values of $k_{off}^{(0)}$, F_{d1} and F_{d2} are determined by fitting the available experimental data [46] to equations (8) and (9). As shown in figure 1(c), we have $k_{off}^{(0)} = 1/7.5\ s^{-1}$ and $F_{d1} = F_{d2} = 1.75$ pN (table 1).

2.2. Ndc80 protein

Under no external force, Ndc80 makes an unbiased one-dimensional diffusion on MT [16, 17]. We still denote by ε_0 the potential energy of Ndc80 in the initial position, by ε_1 the potential energy after Ndc80 takes the forward step and by ε_{-1} the potential energy after Ndc80 takes the backward step. As done in the literature [15, 56], the forward and backward stepping rates can be written as

$$k_F^{(Ndc)} = k_0^{(Ndc)} \exp\left[\beta\lambda(\varepsilon_0 - \varepsilon_1)\right], \tag{10}$$

$$k_B^{(Ndc)} = k_0^{(Ndc)} \exp\left[\beta\lambda(\varepsilon_0 - \varepsilon_{-1})\right], \tag{11}$$

where $k_0^{(Ndc)}$ is the stepping rate under no external force, namely with $\varepsilon_0 = \varepsilon_1 = \varepsilon_{-1}$. As determined experimentally before [17], under no external force the diffusion constant of the single Ndc80 is about $D = 0.085\ \mu m^2\ s^{-1}$. From the relation, $D = k_0^{(Ndc)} d^2$, we have $k_0^{(Ndc)} = 1264\ s^{-1}$. For simplicity, we take $\lambda = 0.5$ for Ndc80.

In the main text, we do not consider the detachment of Ndc80. In supplementary information (section S1 (available online at stacks.iop.org/CTP/74/105601/mmedia)) we consider the detachment of Ndc80. The detachment rate of Ndc80 versus the external force F also has the single-exponential form, as described by equations (8) and (9), where we take $F_{d1} = F_{d2} = F_d$. As done in [17], we take $k_{off}^{(0)} = 2\ s^{-1}$ and $F_d = 20$ pN.

3. Results

3.1. The kinesin stalk can rotate freely in a large range of the angle relative to its head

Due to the flexibility of the NL, it is argued here that the relatively rigid rod-like stalk that connects the two heads via their NLs can rotate freely in a large range of angle relative to the heads. To validate this argument, we resort to all-atom MD simulations (see Methods section). The system for our MD simulations is the x-ray structure of the single kinesin head (pdb: 2KIN) [57]. The structure of 2KIN is composed of a motor domain with the docked NL and an α7 helix that can form the coiled-coil stalk with that of the partner head.

We perform MD simulations of the system for a time of 250 ns (see movie S1 in supplementary information). In figures 2(a)–(d) we show some snapshots of the structure at different simulation times, and in figure 2(e) we show the temporal evolution of the angles of the helix relative to the three planes, *y'o'z'*, *x'o'y'* and *x'o'z'*, that are fixed relative to the head. From figure 2 and movie S1 it is seen that indeed the α7 helix can rotate freely in a large range of the angle relative to the head. The rotation of the α7 helix relative to the head is equivalent to that of the stalk relative to the two heads of the motor in the dimeric form. This large rotation of the stalk can have a large effect on the cargo transport by multiple kinesin motors and MAPs.

3.2. Velocity of cargo driven by multiple kinesin motors of truncated stalks

As shown in the above section, the stalk of the kinesin motor can rotate freely in a large range of angle relative to the two heads. This implies that for a cargo driven by multiple kinesin motors moving on an MT filament, as schematically shown in figure 3, when the angle of the stalk of a motor (e.g. motor 2)

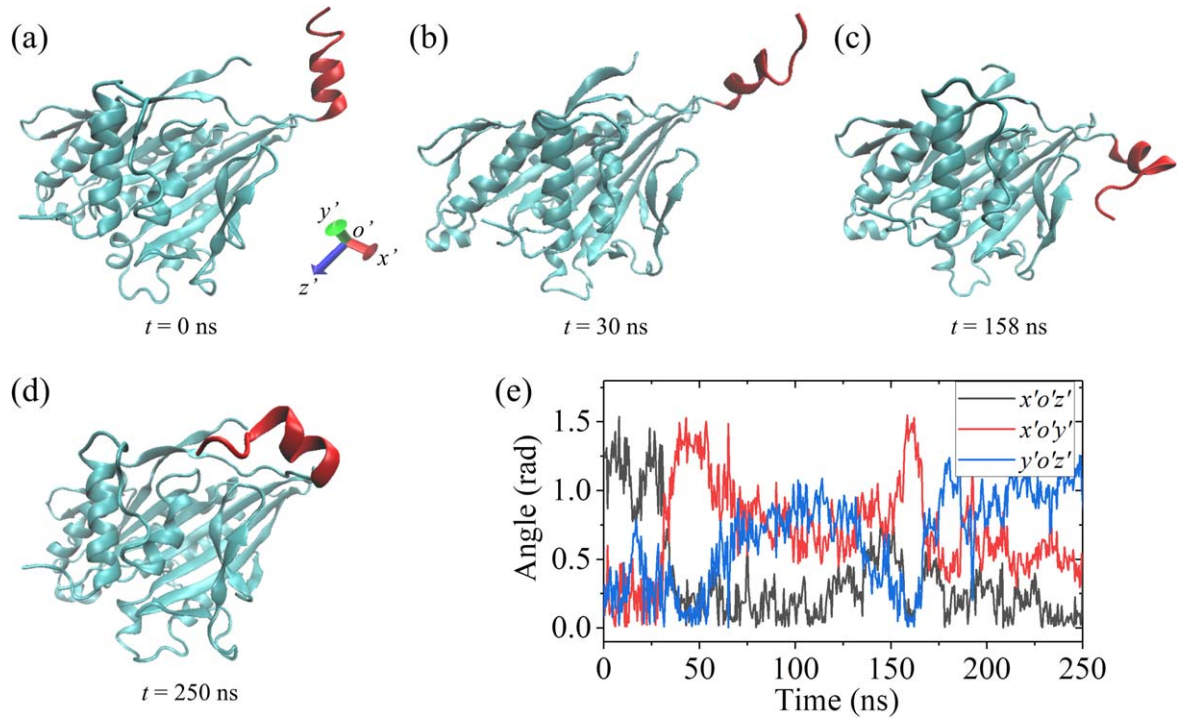

Figure 2. All-atom MD simulation results for the kinesin head with a segment of $\alpha 7$ helix. (a)–(d) Structures at different simulation times, with $t = 0$ corresponding to the initial simulation time. The head is drawn in cyan and the $\alpha 7$ helix is drawn in red. (e) Temporal evolution of the angle of the $\alpha 7$ helix relative to the three planes, *y'o'z'*, *x'o'y'* and *x'o'z'*.

relative to the y axis in xoy plane is in a range of $-\theta_0 < \theta < \theta_0$, within which the stalk can rotate freely, the motor can move freely on the MT filament in a range of $-l_0 < x < l_0$, within which its stalk is not stretched. In other words, during the processive stepping in the range of $-l_0 < x < l_0$ the motor experiences no external force. By contrast, if the angle of the stalk of a motor (e.g. motor 1 or motor 3) relative to the y axis in xoy plane is smaller than $-\theta_0$ or larger than θ_0, namely with $|x| > l_0$, the motor experiences the external force of the magnitude of $K_1(|x| - l_0)$ arising from the stretching of the stalk, where K_1 is the spring coefficient of the stalk. Under this consideration, we study numerically the cooperative transport of the cargo by multiple kinesin motors in this section. We use both the constant-force model and the varying-force model.

The simulation methods are described in the Methods section. The parameter values for the kinesin motors are listed in table 1. After detachment from MT, the rebinding rate of the kinesin-1 motor is taken as $\mu = 5\ \mathrm{s}^{-1}$ (table 1), which is consistent with the available experimental data [58], and the rebinding rate of the CENP-E motor is taken as $\mu = 0.4\ \mathrm{s}^{-1}$ (table 1), as taken before [17]. The spring coefficient of the stalk, K_1, is chosen as follows. In the full-length form, kinesin-1 has a stalk length of about 110 nm [34]. The available experimental data indicated that the spring coefficient of the stalk of the full-length kinesin-1 is about 0.3 pN nm^{-1} [52]. In the experiments of Chakraborty *et al* [17], the truncated kinesin-1 motors, CENP-1 motors and Ndc80 proteins of the stalk length of about 30 nm were used. Here, we also consider the truncated kinesin motors having a stalk length of 30 nm. The spring coefficient of the truncated kinesin-1 and CENP-E is then estimated to be about 1.1 pN nm^{-1}. Thus, we take $K_1 = 1$ pN nm^{-1} in the calculation.

First, we use the constant-force model, namely, we use equation (1) to calculate the forward stepping rate of one motor. In figure 4(a) (left panel) we show the calculated results of the velocity of the cargo driven by multiple kinesin-1 motors versus the number, N, of the motors connected to the cargo for different values of l_0. In some prior theoretical and numerical studies [27–29], it was considered that no range on the MT filament is present, in which the motors can step freely without experiencing any external force. The results with $l_0 = 0$ shown in figure 4(a) correspond to the case of those prior studies. For comparison, the available experimental data on the velocity versus the number of kinesin-1 motors are shown in the right panel of figure 4(a) [25]. The corresponding calculated results for CENP-E are shown in figure 4(b) (left panel). For comparison, the available experimental data on the velocity versus the concentration of CENP-E motors are shown in the right panel of figure 4(b) [26]. From figure 4(a) (left panel) it is seen that for any value of l_0, the calculated velocity of the cooperative transport by multiple kinesin-1 motors increases slightly with the increase of the motor number N. From figure 4(b) (left panel) it is seen that for any value of l_0, the calculated velocity of the cooperative transport by multiple CENP-E motors is insensitive to the motor number N. By contrast, the experimental data (right panel of figure 4(b)) showed that the velocity of the cooperative transport by multiple CENP-E motors decreases evidently with the increase of the motor concentration and becomes leveled off at high motor concentrations [26] (noting that the velocity becoming leveled off at high motor

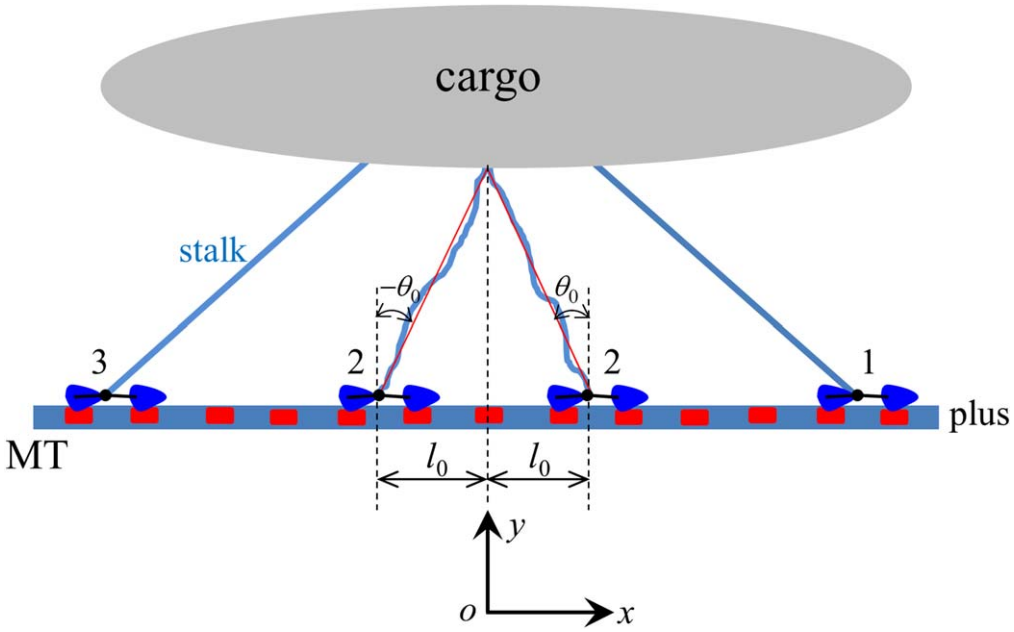

Figure 3. Schematic diagram of the cargo driven by three kinesin motors. When the angle of the stalk of a motor (e.g. motor 2) relative to the y axis in xoy plane is in the range of $-\theta_0 < \theta < \theta_0$, within which the stalk of the motor is not stretched, the motor can move freely on the MT filament in the range of $-l_0 < x < l_0$ without experiencing the external force arising from the stretching of the stalk. Here, motor 2 is drawn in two different positions, with one at $x = -l_0$ and the other at $x = l_0$. When the angle of the stalk of a motor (e.g. motor 1 or motor 3) relative to the y axis in xoy plane is smaller than $-\theta_0$ or larger than θ_0, the motor experiences the external force arising from the stretching of the stalk.

concentrations implies that the decrease of the velocity does not arise from crowding of the motors). The inconsistency between the numerical and experimental results of CENP-E motors indicates that the constant-force model is not reasonable.

Second, we use the varying-force model, namely, we use equation (4) to calculate the forward stepping rate of the moving motor. The free energy change $\varepsilon_1 - \varepsilon_0$ in equation (4) corresponds to the change in the total elastic energy of stretching of all stalks of the motors when the moving motor takes one step because the stepping of the motor is required to stretch all stalks of the motors involved. In figure 5(a) (left panel) we show the calculated results of the velocity of the cargo by multiple kinesin-1 motors versus the motor number N for different values of l_0. For comparison, the available experimental data on the velocity versus the number of kinesin-1 motors are shown in the right panel of figure 5(a) [25]. From figure 5(a) (left panel) it is seen that with $l_0 = 0$ the velocity decreases evidently with the increase of the motor number. Interestingly, with $l_0 \geqslant d$, the velocity of the cargo is insensitive to the motor number. This implies that for the cooperative transport by multiple kinesin-1 motors, the presence of a range in which the motors can step freely without experiencing any external force has the advantage over the absence of such a range. The corresponding calculated results for CENP-E are shown in figure 5(b) (left panel). For comparison, the available experimental data on the velocity versus the concentration of the CENP-E motors are shown in the right panel of figure 5(b) [26]. From figure 5(b) (left panel) it is seen that with $l_0 = 0$ the velocity decreases largely with the increase of the motor number. With $l_0 \geqslant d/2$ the velocity at large N has a much smaller decrease relative to that at $N = 1$ than with $l_0 = 0$. The larger the l_0 is, the smaller the velocity decreases. This implies that for the cooperative transport by multiple CENP-E motors, the presence of a range in which the motors can step freely without experiencing any external force also has the advantage over the absence of such a range. More interestingly, from figure 5 it is seen that for both the cooperative transport by kinesin-1 motors and that by CENP-E motors, the calculated results on the curve form of velocity versus N with $l_0 = d$ (red dots in the left panels) are in good agreement with the experimental results. Speaking concretely, for the kinesin-1 motors, both the calculated velocity with $l_0 = d$ and the experimental velocity are kept nearly unchanged with the change of the motor number or concentration. Note that by tuning parameter $k^{(+)}$ (with $k^{(+)} = 85$ s^{-1}) while keeping other parameters unchanged for the kinesin-1 motors we can make the calculated velocity (with $l_0 = d$) be in quantitative agreement with the experimental data (see figure S2 in supplementary information). For the CENP-E motors, both the calculated velocity with $l_0 = d$ at $N = 1$ and that at large N are in quantitative agreement with the experimental velocity at $N = 1$ or at the very low motor concentration and that at the high motor concentration, respectively. These results support strongly the varying-force model.

Taken together, the studies in this section show that the varying-force model is more reasonable than the constant-force model to describe the cooperative transport by multiple kinesin motors. Thus, in the following studies, we will only use the varying-force model.

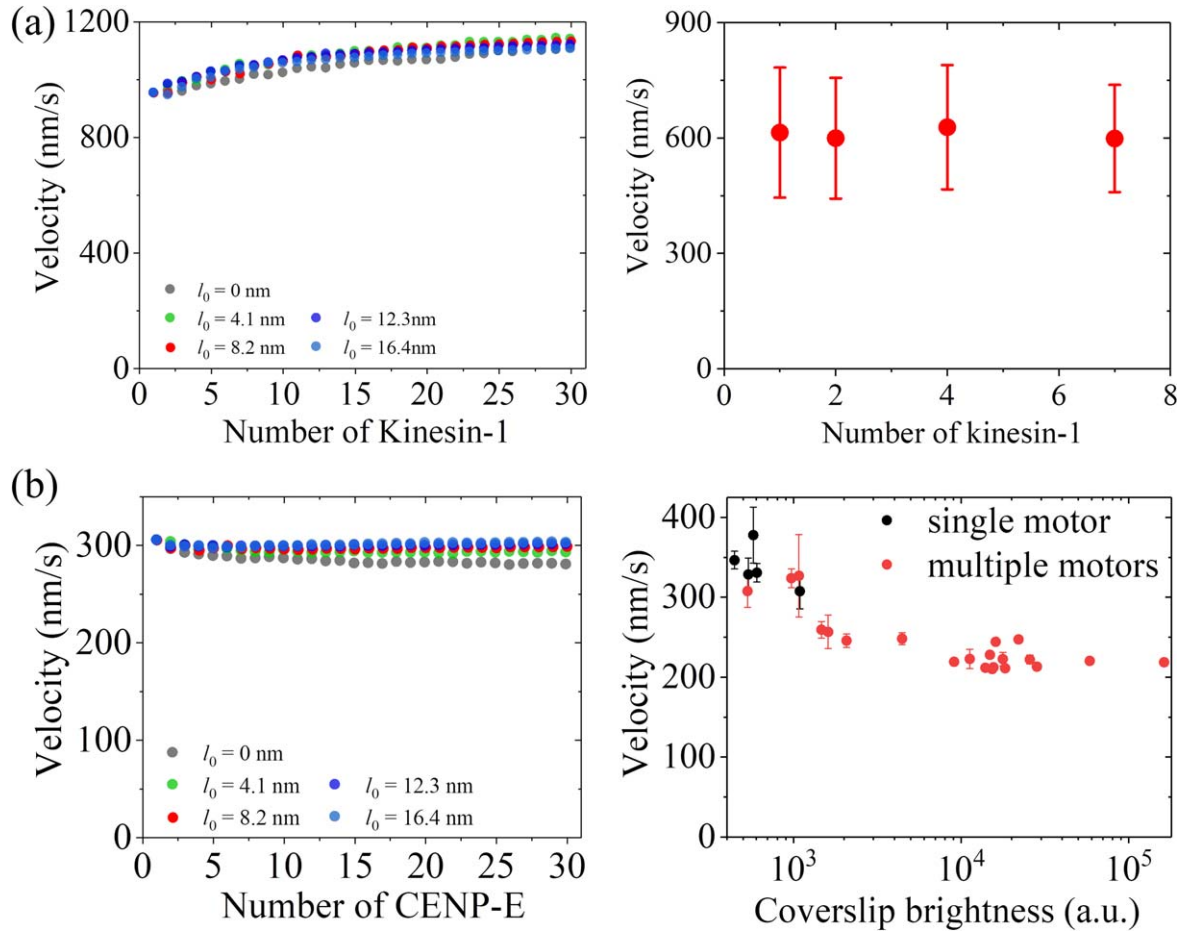

Figure 4. Results for velocity of cooperative transport by multiple kinesin motors of the truncated stalks studied with the constant-force model. (a) The results for the case of kinesin-1 motors. The left panel shows the calculated velocity versus the number of motors connected to the cargo for different values of l_0. The right panel shows the experimental data taken from Derr *et al* [25]. (b) The results for the case of CENP-E motors. The left panel shows the calculated velocity versus the number of motors connected to the cargo for different values of l_0. The right panel shows the experimental data taken from Chakraborty *et al* [26].

3.3. Velocity of cargo driven by multiple kinesin motors and Ndc80 proteins of truncated stalks

In this section, we study the cooperative cargo transport by multiple kinesin motors and Ndc80 proteins with truncated stalks of the length of 30 nm, as done in the experiments of Chakraborty *et al* [17] Thus, we take the spring coefficient $K_2 = 1$ pN nm^{-1} for Ndc80 proteins having the same value as $K_1 = 1$ pN nm^{-1} for motors, as done in the above section. For the motor, we consider that there is a range of $-l_0 < x < l_0$ on the MT filament, in which the motor can step freely without experiencing any external force. Different from the structure of the kinesin motor, showing that the connection between the stalk and head is flexible, the structure of Ndc80 protein indicated that the connection between the stalk and head is not flexible [59–61]. Thus, for the Ndc80 protein, there is no range on the MT filament, in which the protein can diffuse freely without experiencing any external force. We use the varying-force model here. As discussed in the above section, the energy changes $\varepsilon_1 - \varepsilon_0$ and $\varepsilon_{-1} - \varepsilon_0$ in equations (4), (10) and (11) correspond to the change in the total elastic energy of stretching of all stalks of the motors and Ndc80 proteins when the moving motor or Ndc80 takes one step. The simulation methods are described in the Methods section. The parameter values for the kinesin motors are given in table 1. The parameter values for Ndc80 are $k_0^{(\mathrm{Ndc})} = 1264$ s^{-1} and $\lambda = 0.5$, as mentioned above. For simplicity, the detachment of Ndc80 is not considered here. In the system, the number of motors connected to the cargo, N, is kept fixed while the number of Ndc80 proteins connected to the cargo is varied, and thus the ratio of Ndc80 to kinesin-1 number is varied, as done in the experiments of Chakraborty *et al* [17]. As the available experimental data indicated about 8–30 Ndc80 complexes per microtubule at kinetochores [20, 62, 63], we take $N = 9$, 15, 24, 30 in our calculations.

In figures 6(a)–(c), we show the calculated results of the velocity of the cargo driven by multiple kinesin-1 motors and Ndc80 proteins versus the ratio of Ndc80 to kinesin-1 number for different values of l_0 and different kinesin-1 number N, where the velocity is normalized by the velocity in the absence of Ndc80 with the same N. The corresponding results for cargo transport by multiple CENP-E motors and Ndc80 proteins are shown in figures 6(d)–(f). For comparison, in figure 6 we also show the corresponding experimental data measured by Chakraborty *et al* [17]. From figure 6 it is seen

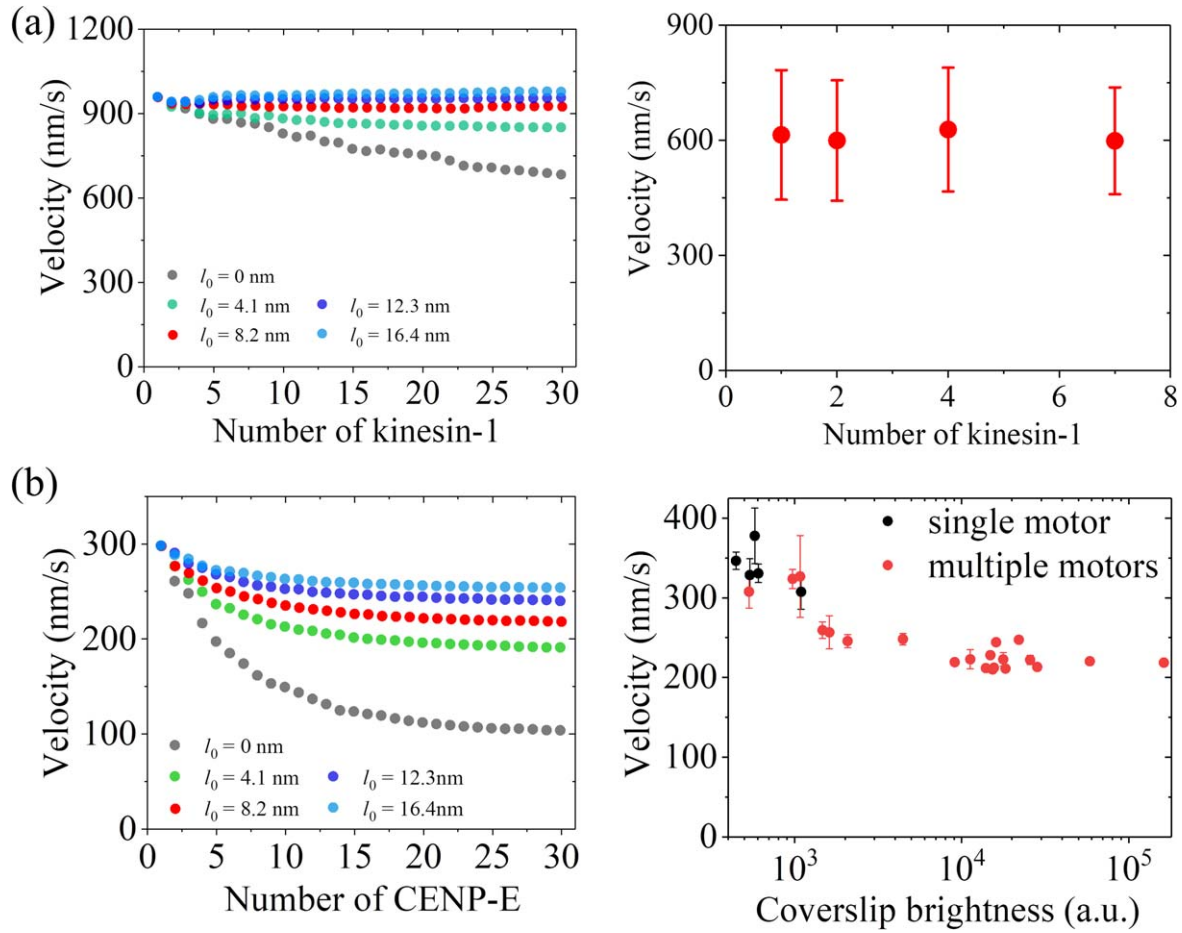

Figure 5. Results for velocity of cooperative transport by multiple kinesin motors of the truncated stalks studied with the varying-force model. (a) The results for the case of kinesin-1 motors. The left panel shows the calculated velocity versus the number of motors connected to the cargo for different values of l_0. The right panel shows the experimental data taken from Derr *et al* [25]. (b) The results for the case of CENP-E motors. The left panel shows the calculated velocity versus the number of motors connected to the cargo for different values of l_0. The right panel shows the experimental data taken from Chakraborty *et al* [26].

interestingly that the results for the normalized velocity are insensitive to l_0. This can be understood as follows. Although at a given ratio of Ndc80 to motor number the cargo velocity by multiple motors and Ndc80 proteins increases with the increase of l_0, the cargo velocity by multiple motors in the absence of Ndc80 also increases with the increase of l_0 (see figure 5(b)). This thus gives the normalized velocity at a given ratio of Ndc80 to motor number to be insensitive to l_0. More interestingly, from figures 6(a)–(c) it is seen that for the case of cargo transport by multiple kinesin-1 motors and Ndc80 proteins, the results are in good agreement with the experimental data for any N ($\geqslant$9). When the ratio of Ndc80 to kinesin-1 number becomes equal to one, implying that both the motors and Ndc80 proteins have the same number, the cargo velocity is reduced by about 5-fold relative to that when the ratio of Ndc80 to kinesin-1 number is equal to zero, implying that only the motors are present. From figures 6(d)–(f) it is seen that for the case of cargo transport by multiple CENP-E motors and Ndc80 proteins, the results are in good agreement with the experimental data when $N \geqslant 24$. When the ratio of Ndc80 to CENP-E number becomes equal to one, namely both the motors and Ndc80 proteins having the same number, the cargo velocity becomes nearly equal to zero. The underlying mechanism of the sensitive decrease in the velocity to the increase in the ratio of Ndc80 to kinesin number is as follows. Since the short truncated stalks for both motors and Ndc80 proteins have the large spring coefficients K_1 and K_2, the energy change $\varepsilon_1 - \varepsilon_0$ caused by the forward stepping of the moving motor is large, thus resulting in a large decrease in the forward stepping rate of the motor, as noted from equation (4).

In addition, it is noted that at a given ratio of Ndc80 to CENP-E number the normalized velocity for $l_0 = d = 8.2$ nm (figure 6(d)) is very similar to that for $l_0 = 2d = 16.4$ nm (figure 6(f)). Moreover, it is noted that at a given ratio of Ndc80 to CENP-E number the difference between the normalized velocity for $l_0 = d = 8.2$ nm (figure 6(d)) and that for $l_0 = 3d/2 = 12.3$ nm (figure 6(e)) is larger than the difference between the normalized velocity for $l_0 = d = 8.2$ nm (figure 6(d)) and that for $l_0 = 2d = 16.4$ nm (figure 6(f)). These results can be understood as follows. Consider that one motor is initially at the equilibrium position $x = 0$ with $\theta = 0$ (see figure 3). For the case of $l_0 = nd$ (n is an integer), during the movement from $x = 0$ to $x = l_0 = nd$ the motor

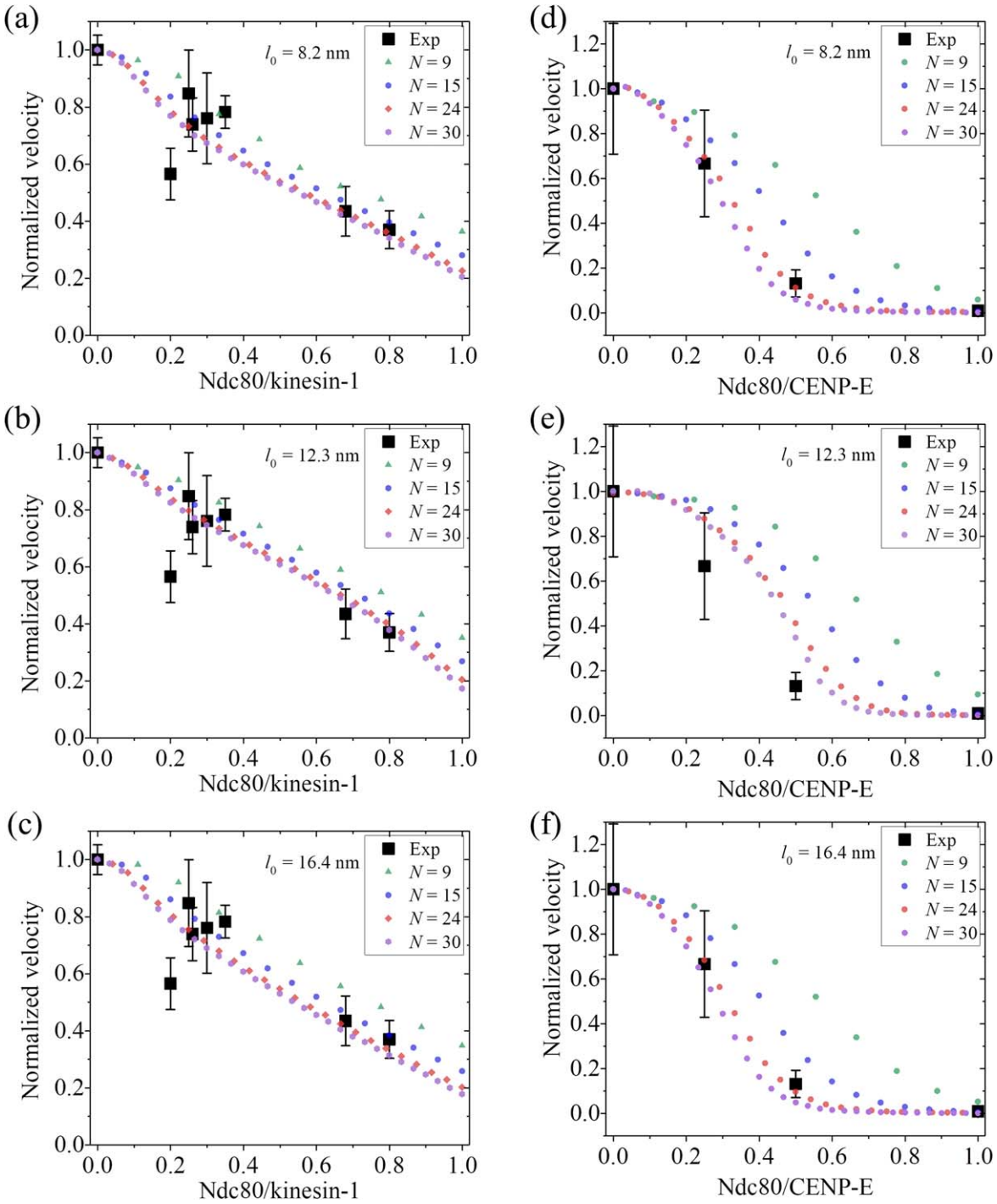

Figure 6. Results for velocity of cooperative transport by multiple kinesin motors and Ndc80 proteins of the truncated stalks studied with the varying-force model. The experimental data are taken from Chakraborty *et al* [17], with the errors of the experimental data being calculated with $\Delta(v/v_0) = |\partial(v/v_0)/\partial v|\ \Delta v + |\partial(v/v_0)/\partial v_0|\ \Delta v_0$, where v and v_0 denote the velocities with the presence and absence of Ndc80 proteins, respectively. (a)–(c) The normalized velocity of the cooperative transport by multiple kinesin-1 motors and Ndc80 proteins versus the ratio of Ndc80 to kinesin-1 number for different values of l_0 and different kinesin-1 number N, where the velocity is normalized by the velocity in the absence of Ndc80 with the same N. (d)–(f) The normalized velocity of the cooperative transport by multiple CENP-E motors and Ndc80 proteins versus the ratio of Ndc80 to CENP-E number for different values of l_0 and different CENP-E number N, where the velocity is normalized by the velocity in the absence of Ndc80 with the same N.

experiences no force arising from the stretching of the stalks of the motor and Ndc80, while throughout the next whole step from $x = l_0 = nd$ to $x = (n+1)d$ the movement of the motor is affected by the energy change arising from the stretching of the stalks of the motor and Ndc80. Thus, it is approximately expected that for any n the normalized velocity of the cargo is very similar. By contrast, for the case of $l_0 = (n+1/2)d$, during the movement from $x = 0$ to $x = l_0 = (n+1/2)d$ the motor experiences no force arising from the stretching of the stalks of the motor and Ndc80, while throughout the next half

step from $x = (n+1/2)d$ to $x = (n+1)d$ the movement of the motor is affected by the energy change arising from the stretching of the stalks of the motor and Ndc80. Thus, it is approximately expected that the difference between the normalized velocity for $l_0 = d$ (figure 6(d)) and that for $l_0 = 3d/2$ (figure 6(e)) is larger than the difference between the normalized velocity for $l_0 = d$ (figure 6(d)) and that for $l_0 = 2d$ (figure 6(f)).

It is noted that for simplicity we have not considered the detachment of the Ndc80 protein in figure 6. With the consideration of the detachment of the Ndc80 protein, the calculated results are also in good agreement with the experimental data (see section S1 in supplementary information).

3.4. Velocity of cargo driven by multiple kinesin motors and Ndc80 proteins of full-length stalks

In this section, we make similar studies to those presented in the above section except that we use the full-length kinesin motors and Ndc80 proteins. Thus, we take $K = 0.3$ pN nm^{-1} for the full-length kinesin-1 motors, as mentioned above. Since the full-length CENP-E has a length of about 200–230 nm [64], we take $K_1 = 0.15$ pN nm^{-1} for CENP-E motors. Since the full-length Ndc80 has a length of about 60 nm [57, 65], we take $K_2 = 0.55$ pN nm^{-1} for Ndc80 proteins. For simplicity, we take the truncated and full-length kinesin motors having the same values for other parameters, as used in the above section.

In figures 7(a)–(c), we show the calculated results of the velocity of the cargo driven by multiple full-length kinesin-1 motors and Ndc80 proteins versus the ratio of Ndc80 to kinesin-1 number for different values of l_0 and different kinesin-1 number N, where the velocity is normalized by the velocity in the absence of Ndc80 with the same N. The corresponding results for cargo transport by multiple full-length CENP-E motors and Ndc80 proteins are shown in figures 7(d)–(f). From figure 7 it is seen interestingly that the velocity decreases only slowly with the increase in the ratio of Ndc80 to kinesin number, which is contrary to the case of the kinesin motors of the truncated stalks (figure 6). The small decrease of the velocity for the case of full-length stalks is due to the small elastic energy change $\varepsilon_1 - \varepsilon_0$ when one motor takes a forward step, which is in turn due to the small spring coefficients K_1 and K_2 of the stalks for both motors and Ndc80 proteins. Thus, the kinesin motors in the full-length form, together with MAPs, can transport cargo much more efficiently than the truncated ones with the shorter stalk length. This gives an explanation of why the full-length kinesin motor, and in particular the CENP-E motor, has a long stalk.

4. Discussion

In some prior theoretical and numerical studies of cargo transport by multiple kinesin motors [27–29], it was assumed that there is an equilibrium position of one motor on MT, at which the stalk of the motor is not stretched and thus the motor experiences no external force. However, no range for the equilibrium position of the motor is present, within which the stalk of the motor is not stretched and thus the motor can step freely without experiencing any external force. On the contrary, the all-atom MD simulations here indicate that the stalk of the kinesin motor can rotate freely in a large range of the angle relative to the head (figure 2 and Movie S1). This implies that for the cargo transport by multiple kinesin motors and MAPs, a range for the equilibrium position of a motor is present, within which the stalk of the motor is not stretched and thus the motor can step freely without experiencing any external force, as argued in other prior studies [30–36]. The studies here show that the presence of the range of the equilibrium position has an advantage over the absence of such the range in the cooperative transport of the cargo by multiple motors, with the velocity of the cargo for the former being larger than that for the latter (figure 5).

In prior theoretical and numerical studies of cargo transport by multiple kinesin motors [27, 28, 34–41], the force dependence of the velocity for the single motor was generally described by the constant-force model, in which it was assumed that during the moving period in one step the motor experiences the constant external force F that is equal to that during the dwell period before the moving period. The studies here show that with the constant-force model for the single motor, the calculated results of the velocity of the cargo transport by multiple CENP-E motors versus the motor number or concentration are inconsistent with the available experimental data (figure 4). Recently, the varying-force model was used to study the dynamics of the single motor in the single molecule optical trapping experiments, in which it was proposed that during the moving period in one step the motor experiences the varying external force although during the dwell period the motor experiences the constant external force [32, 47]. Here, with the varying-force model for the motor, both the calculated results on the motor-number dependence of the velocity of the cargo transport by multiple kinesin-1 motors and those by multiple CENP-E motors are in good agreement with the available experimental data (figure 5).

It is noted that for the cargo transport by multiple kinesin motors and Ndc80 proteins with the truncated stalks, the cargo velocity decreases significantly with the increase of the ratio of Ndc80 to kinesin number. For example, in the case of kinesin-1, when the ratio is 0.8 the cargo velocity normalized by that with the ratio equal to zero is only about 0.37 (figure 6). For the case of CENP-E, when the ratio is 1 the cargo velocity becomes nearly zero (figure 6). Here, we give a quantitative explanation of these results. These results indicate that when the ratio of Ndc80 to kinesin number is high the cargo transport is very inefficient. In particular, when the ratio of Ndc80 number to CENP-E number is 1, the cargo is unable to be transported. Interestingly, we show that the velocity of the cargo transport by multiple kinesin motors and Ndc80 proteins with the full-length stalks decreases only slowly with the increase of the ratio of Ndc80 to kinesin number (figure 7). In particular, even when the ratio of Ndc80 to CENP-E number is 1, the cargo velocity is decreased by only about 1.2-fold,

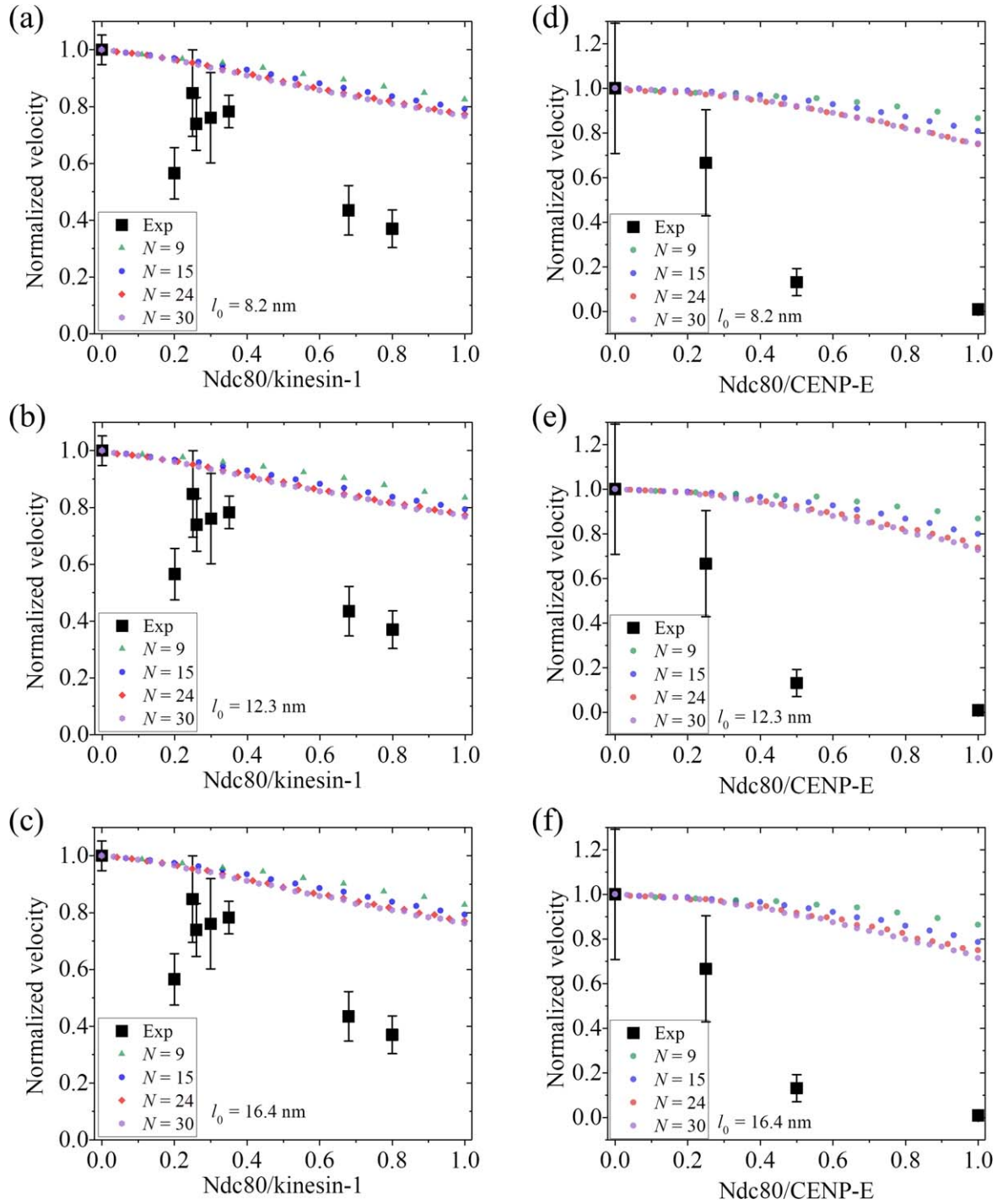

Figure 7. Results for velocity of cooperative transport by multiple kinesin motors and Ndc80 proteins of the full-length stalks studied with the varying-force model. For comparison, the experimental data that are the same as those shown in figure 6 are reshown here. (a)–(c) The normalized velocity of the cooperative transport by multiple kinesin-1 motors and Ndc80 proteins versus the ratio of Ndc80 to kinesin-1 number for different values of l_0 and different kinesin-1 number N, where the velocity is normalized by the velocity in the absence of Ndc80 with the same N. (d)–(f) The normalized velocity of the cooperative transport by multiple CENP-E motors and Ndc80 proteins versus the ratio of Ndc80 to CENP-E number for different values of l_0 and different CENP-E number N, where the velocity is normalized by the velocity in the absence of Ndc80 with the same N.

implying a very efficient cargo transport. This thus gives an explanation of why CENP-E has a long stalk.

In conclusion, using the varying-force model and with the argument of the presence of the range of the equilibrium position of the motor on MT, which is verified by our all-atom MD simulations, our calculated results for the velocity in the cooperative transport by multiple kinesin motors versus the motor number reproduce well the available experimental data. Moreover, we study numerically the cooperative cargo transport by multiple kinesin motors and Ndc80 proteins with

the truncated stalks of the large spring coefficient, explaining quantitatively the available experimental results on the velocity versus the ratio of Ndc80 to kinesin number. The sensitive decrease of the velocity to the ratio of Ndc80 to motor number is due to the large decrease of the forward stepping rate of the moving motor, which arises from the large change in the elastic potential energy of stretching the stalks of the motors and Ndc80 proteins when the moving motor makes a forward stepping. The cooperative cargo transport by multiple kinesin motors and Ndc80 proteins with the full-length stalks of the small spring coefficient is also studied numerically. The results show that the velocity of the cargo decreases only slowly with the increase in the ratio of Ndc80 to kinesin number. This is due to the small change in the elastic potential energy of stretching the stalks of the motors and Ndc80 proteins when the moving motor makes a forward stepping. Our results thus give an explanation of why the full-length kinesin motor, and in particular the CENP-E motor, has a long stalk. The predicted results with the full-length stalks can be easily tested by future experiments.

5. Methods

5.1. All-atom MD simulations

We use the structure of the single rat kinesin head (pdb: 2KIN) [57] as the starting model in our all-atom MD simulations. The MD simulation procedure is described in detail in our previous works [66, 67], which is re-described briefly here. The missing atoms in the structure are added by using the software Swiss-PdbViewer. Counter-ions are added to neutralize the system. The kinesin head is solvated in a water box (using the TIP3P water model [68]). In our simulations, the distance between the protein complex and the boundary of the box is about 4 nm to avoid the edge effect. The MD simulations are run in Gromacs4.6 [69] using the AMBER99SB force field [70] with a time step of 2 fs. All chemical bonds are constrained using the LINCS algorithm [71]. The cutoff for van der Waals interaction and short-range electrostatics interaction is set as 1.4 nm. The long-range electrostatic interaction is calculated using the particle mesh Ewald (PME) algorithm [72]. Velocity-rescaling temperature coupling [73] and Berendsen pressure coupling [74] are used. We first perform the energy minimizations twice. The energy minimizations are performed for 5×10^4 steps using the steepest descent method. Then the systems are equilibrated for 100 ps at 300 K and 1 bar pressure in the NVT ensemble and NPT ensemble, respectively. In the MD simulations, we restrict residues 223–227 in the head. These restricted residues are far away from the neck so that the restriction of them would have no influence on the motion of the neck domain. The simulated results are analyzed by VMD1.9.2 [75].

5.2. Monte-Carlo simulations

The Monte-Carlo simulation procedure is described in detail in our previous works [28, 39, 44], which is re-described briefly here. In our simulations, we take the time step $h = 10^{-5}$ s. we have checked that doubling the time step h has no effect on our results. For each kinesin motor connected to the cargo, we take 4 independent random numbers uniformly distributed between 0 and 1, *ran*1, *ran*2, *ran*3, and *ran*4. During each time step h, if $ran1 < k_F^{(M)}h$ the motor bound to MT takes a forward step. If $ran2 < k_B^{(M)}h$ the motor bound to MT takes a backward step. If $ran3 < k_{off}h$ the motor bound to MT detaches from the MT. When the motor is detached from MT, if $ran4 < \mu h$, the motor rebinds to the MT. It is noted that in a one-time step with a very small size 10^{-5} s, of the four conditions $ran1 < k_F^{(M)}h$, $ran2 < k_B^{(M)}h$, $ran3 < k_{off}h$ and $ran4 < \mu h$ more than one condition that can be satisfied can occur with a very small probability. If in a one-time step more than one condition can be satisfied, the related events are considered to occur in an ordered sequence. For example, if in one time step both $ran1 < k_F^{(M)}h$ and $ran3 < k_{off}\,h$ are satisfied, we consider that the motor takes a forward step and then detaches from the MT. If in one time step both $ran3 < k_{off}\ h$ and $ran4 < \mu h$ are satisfied, we consider that the motor detaches from the MT and then rebinds to the MT, which is equivalent to that no detaching and rebinding events occur.

For each Ndc80 connected with the cargo, we also take 4 independent random numbers uniformly distributed between 0 and 1, *ran*5, *ran*6, *ran*7, and *ran*8. During each time step h, if $ran5 < k_F^{(Ndc)}h$ the Ndc80 takes a forward step. If $ran6 < k_B^{(Ndc)}h$ the Ndc80 takes a backward step. If $ran7 < k_{off}\,h$ the Ndc80 bound to MT detaches from the MT. When the Ndc80 is detached from MT, if $ran8 < \mu h$, the Ndc80 rebinds to the MT. It is noted that in a one-time step with a very small size 10^{-5} s, of the four conditions $ran5 < k_F^{(Ndc)}h$, $ran6 < k_B^{(Ndc)}h$, $ran7 < k_{off}h$ and $ran8 < \mu h$ more than one condition that can be satisfied can occur with a very small probability. If in a one-time step more than one condition can be satisfied, the related events are also considered to occur in an ordered sequence, as mentioned above for the motor.

With the above-mentioned Monte-Carlo simulation procedure, the method for simulations of the cargo transport by multiple kinesin motors and Ndc80 proteins is described in the supplementary information (section S2). With the varying-force model for kinesin motors, the method to calculate the stepping rate of one motor in the cargo transport by multiple kinesin motors and Ndc80 proteins is described in the supplementary information (section S3). The method to calculate the stepping rate of one Ndc80 protein in the cargo transport by multiple kinesin motors and Ndc80 proteins is also described in the supplementary information (section S3).

ORCID iDs

Yao Wang https://orcid.org/0000-0002-4241-4100
Yu-Ru Liu https://orcid.org/0000-0001-9318-7617
Peng-Ye Wang https://orcid.org/0000-0002-9765-0610
Ping Xie https://orcid.org/0000-0003-1485-6355

References

[1] Vale R D 2003 The molecular motor toolbox for intracellular transport *Cell* **112** 467–80

[2] Hirokawa N, Noda Y, Tanaka Y and Niwa S 2009 Kinesin superfamily motor proteins and intracellular transport *Nat. Rev. Mol. Cell Bio.* **10** 682–96

[3] Howard J 1996 The movement of kinesin along microtubules *Annu. Rev. Physiol.* **58** 703–29

[4] Hirokawa N 1998 Kinesin and dynein superfamily proteins and the mechanism of organelle transport *Science* **279** 519–26

[5] Cross R A 2004 The kinetic mechanism of kinesin *Trends Biochem. Sci* **29** 301–9

[6] Holzbaur E L and Goldman Y E 2010 Coordination of molecular motors: from *in vitro* assays to intracellular dynamics *Curr. Opin. Cell Biol.* **22** 4–13

[7] Monroy B Y, Sawyer D L, Ackermann B E, Borden M M, Tan T C and Ori-McKenney K M 2018 Competition between microtubule-associated proteins directs motor transport *Nat. Commun.* **9** 1487

[8] Pringle J, Muthukumar A, Tan A, Crankshaw L, Conway L and Ross J L 2013 Microtubule organization by kinesin motors and microtubule crosslinking protein MAP65 *J. Phys. Condens. Matter* **25** 374103

[9] Amin M A, McKenney R J and Varma D 2018 Antagonism between the dynein and Ndc80 complexes at kinetochores controls the stability of kinetochore–microtubule attachments during mitosis *J. Biol. Chem.* **293** 5755–65

[10] Chaudhary A R, Lu H, Krementsova E B, Bookwalter C S, Trybus K M and Hendricks A G 2019 MAP7 regulates organelle transport by recruiting kinesin-1 to microtubules *J. Biol. Chem.* **294** 10160–71

[11] Azzam O A, Trussell C L and Reinemann D N 2021 Measuring force generation within reconstituted microtubule bundle assemblies using optical tweezers *Cytoskeleton* **78** 111–25

[12] Lopez L A and Sheetz M P 1993 Steric inhibition of cytoplasmic dynein and kinesin motility by MAP2 *Cell Motil. Cytoskeleton* **24** 1–16

[13] Schmidt J C *et al* 2012 The kinetochore-bound Ska1 complex tracks depolymerizing microtubules and binds to curved protofilaments *Dev. Cell* **23** 968–80

[14] Al-Bassam J, Kim H, Brouhard G, van Oijen A, Harrison S C and Chang F 2010 CLASP promotes microtubule rescue by recruiting tubulin dimers to the microtubule *Dev. Cell* **19** 245–58

[15] Lansky Z, Braun M, Lüdecke M, Schlierf M, Ten Wolde P R, Janson M E and Diez S 2015 Diffusible crosslinkers generate directed forces in microtubule networks *Cell* **160** 1159–68

[16] Umbreit N T, Gestaut D R, Tien J F, Vollmar B S, Gonen T, Asbury C L and Davis T N 2012 The Ndc80 kinetochore complex directly modulates microtubule dynamics *Proc. Natl. Acad. Sci. USA* **109** 16113–8

[17] Chakraborty M, Tarasovetc E V, Zaytsev A V, Godzi M, Figueiredo A C, Ataullakhanov F I and Grishchuk E L 2019 Microtubule end conversion mediated by motors and diffusing proteins with no intrinsic microtubule end-binding activity *Nat. Commun.* **10** 1673

[18] Alushin G M, Ramey V H, Pasqualato S, Ball D A, Grigorieff N, Musacchio A and Nogales E 2010 The Ndc80 kinetochore complex forms oligomeric arrays along microtubules *Nature* **467** 805–10

[19] Emanuele M J, Lan W, Jwa M, Miller S A, Chan C S M and Stukenberg P T 2008 Aurora B kinase and protein phosphatase 1 have opposing roles in modulating kinetochore assembly *J. Cell Biol.* **181** 241–54

[20] Joglekar A P, Bouck D, Finley K, Liu X, Wan Y, Berman J, He X, Salmon E D and Bloom K S 2008 Molecular architecture of the kinetochore-microtubule attachment site is conserved between point and regional centromeres *J. Cell Biol.* **181** 587–94

[21] McCleland M L, Gardner R D, Kallio M J, Daum J R, Gorbsky G J, Burke D J and Stukenberg P T 2003 The highly conserved Ndc80 complex is required for kinetochore assembly, chromosome congression, and spindle checkpoint activity *Genes Dev.* **17** 101–14

[22] Civelekoglu-Scholey G and Scholey J M 2010 Mitotic force generators and chromosome segregation *Cell. Mol. Life Sci.* **67** 2231–50

[23] Steblyanko Y, Rajendraprasad G, Osswald M, Eibes S, Jacome A, Geley S, Pereira A J, Maiato H and Barisic M 2020 Microtubule poleward flux in human cells is driven by the coordinated action of four kinesins *EMBO J.* **39** e105432

[24] Maiato H, DeLuca J, Salmon E and Earnshaw W 2004 The dynamic kinetochore-microtubule interface *J. Cell Sci.* **117** 5461–77

[25] Derr N D, Goodman B S, Jungmann R, Leschziner A E, Shih W M and Reck-Peterson S L 2012 Tug-of-war in motor protein ensembles revealed with a programmable dna origami scaffold *Science* **338** 662–5

[26] Chakraborty M, Tarasovetc E V and Grishchuk E L 2018 *In vitro* reconstitution of lateral to end-on conversion of kinetochore–microtubule attachments *Method Cell Biol.* **144** 307–27

[27] Khataee H and Howard J 2019 Force generated by two kinesin motors depends on the load direction and intermolecular coupling *Phys. Rev. Lett.* **122** 188101

[28] Wang Y, Liu Y, Liang J, Wang P and Xie P 2021 Effects of rebinding rate and asymmetry in unbinding rate on cargo transport by multiple kinesin motors *Commun. Theor. Phys.* **73** 15603

[29] Bameta T, Das D, Das D, Padinhateeri R and Inamdar M M 2017 Sufficient conditions for the additivity of stall forces generated by multiple filaments or motors *Phys. Rev.* E **95** 22406

[30] Jamison D K, Driver J W, Rogers A R, Constantinou P E and Diehl M R 2010 Two kinesins transport cargo primarily via the action of one motor: implications for intracellular transport *Biophys. J.* **99** 2967–77

[31] Bouzat S 2016 Models for microtubule cargo transport coupling the Langevin equation to stochastic stepping motor dynamics: Caring about fluctuations *Phys. Rev.* E **93** 12401

[32] Driver J W, Jamison D K, Uppulury K, Rogers A R, Kolomeisky A B and Diehl M R 2011 Productive cooperation among processive motors depends inversely on their mechanochemical efficiency *Biophys. J.* **101** 386–95

[33] Fernández Casafuz A B, De Rossi M C and Bruno L 2020 Intracellular motor-driven transport of rodlike smooth organelles along microtubules *Phys. Rev.* E **101** 62416

[34] kunwar A, Vershinin M, Xu J and Gross S P 2008 Stepping, strain gating, and an unexpected force-velocity curve for multiple-motor-based transport *Curr. Biol.* **18** 1173–83

[35] Berger F, Keller C, Lipowsky R and Klumpp S 2013 Elastic coupling effects in cooperative transport by a pair of molecular motors *Cell. Mol. Bioeng.* **6** 48–64

[36] Arpağ G, Shastry S, Hancock W O and Tüzel E 2014 Transport by populations of fast and slow kinesins uncovers novel family-dependent motor characteristics important for *in vivo* function *Biophys. J.* **107** 1896–904

[37] Uçar M C and Lipowsky R 2020 Collective force generation by molecular motors is determined by strain-induced unbinding *Nano Lett.* **20** 669–76

[38] Muller M J, Klumpp S and Lipowsky R 2008 Tug-of-war as a cooperative mechanism for bidirectional cargo transport by molecular motors *Proc. Natl. Acad. Sci. USA* **105** 4609–14

[39] Fu Y B, Guo S K, Wang P Y and Xie P 2019 Dynamics of cooperative cargo transport by two elastically coupled kinesin motors *Eur. Phys. J.* E **42** 41
[40] Dallon J C, Leduc C, Etienne-Manneville S and Portet S 2019 Stochastic modeling reveals how motor protein and filament properties affect intermediate filament transport *J. Theor. Biol.* **464** 132–48
[41] Portet S, Etienne-Manneville S, Leduc C and Dallon J C 2022 Impact of noise on the regulation of intracellular transport of intermediate filaments *J. Theor. Biol.* **547** 111183
[42] Xie P 2020 Theoretical analysis of dynamics of kinesin molecular motors *ACS Omega* **5** 5721–30
[43] Xie P 2021 Dynamics of kinesin motor proteins under longitudinal and sideways loads *J. Theor. Biol.* **530** 110879
[44] Liu Y, Wang Y, Wang P and Xie P 2021 Effect of kinesin-5 tail domain on motor dynamics for antiparallel microtubule sliding *Int. J. Mol. Sci.* **22** 7857
[45] Andreasson J O L, Milic B, Chen G Y, Guydosh N R, Hancock W O and Block S M 2015 Examining kinesin processivity within a general gating framework *Elife* **4** e07403
[46] Gudimchuk N, Tarasovetc E V, Mustyatsa V, Drobyshev A L, Vitre B, Cleveland D W, Ataullakhanov F I and Grishchuk E L 2018 Probing mitotic CENP-E kinesin with the tethered cargo motion assay and laser tweezers *Biophys. J.* **114** 2640
[47] Xie P 2022 Effect of varying load in moving period of a step on dynamics of molecular motors *Eur. Phys. J.* E **45** 28
[48] Carter N J and Cross R A 2005 Mechanics of the kinesin step *Nature* **435** 308–12
[49] Nishiyama M, Higuchi H and Yanagida T 2002 Chemomechanical coupling of the forward and backward steps of single kinesin molecules *Nat. Cell Biol.* **4** 790–7
[50] Rief M, Rock R S, Mehta A D, Mooseker M S, Cheney R E and Spudich J A 2000 Myosin-V stepping kinetics: a molecular model for processivity *Proc. Natl. Acad. Sci. USA* **97** 9482–6
[51] Clemen A E M, Vilfan M, Jaud J, Zhang J, Bärmann M and Rief M 2005 Force-dependent stepping kinetics of Myosin-V *Biophys. J.* **88** 4402
[52] Coppin C M, Pierce D W, Hsu L and Vale R D 1997 The load dependence of kinesin's mechanical cycle *Proc. Natl. Acad. Sci. USA* **94** 8539
[53] Cao L, Wang W, Jiang Q, Wang C, Knossow M and Gigant B 2014 The structure of apo-kinesin bound to tubulin links the nucleotide cycle to movement *Nat.Commun.* **5** 5364
[54] Xie P 2021 Insight into the chemomechanical coupling mechanism of kinesin molecular motors *Commun. Theor. Phys.* **73** 57601
[55] Xie P 2020 Non-tight and tight chemomechanical couplings of biomolecular motors under hindering loads *J. Theor. Biol.* **490** 110173
[56] Wierenga H and Wolde P R T 2020 Diffusible cross-linkers cause superexponential friction forces *Phys. Rev. Lett.* **125** 78101
[57] Sack S, Muller J, Marx A, Thormahlen M, Mandelkow E M, Brady S T and Mandelkow 1997 X-ray structure of motor and neck domains from rat brain kinesin *Biochemistry* **36** 16155–65
[58] Leduc C, Campas O, Zeldovich K B, Roux A, Jolimaitre P, Bourel-Bonnet L, Goud B, Joanny J F, Bassereau P and Prost J 2004 Cooperative extraction of membrane nanotubes by molecular motors *Proc. Natl. Acad. Sci. USA* **101** 17096–101
[59] Ciferri C, De Luca J, Monzani S, Ferrari K J, Ristic D, Wyman C, Stark H, Kilmartin J, Salmon E D and Musacchio A 2005 Architecture of the human Ndc80-Hec1 complex, a critical constituent of the outer kinetochore *J. Biol. Chem.* **280** 29088–95
[60] Ciferri C *et al* 2008 Implications for kinetochore-microtubule attachment from the structure of an engineered Ndc80 complex *Cell* **133** 427–39
[61] Wilson-Kubalek E M, Cheeseman I M, Yoshioka C, Desai A and Milligan R A 2008 Orientation and structure of the Ndc80 complex on the microtubule lattice *J. Cell Biol.* **182** 1055
[62] Powers A F, Franck A D, Gestaut D R, Cooper J, Gracyzk B, Wei R R, Wordeman L, Davis T N and Asbury C L 2009 The Ndc80 kinetochore complex forms load-bearing attachments to dynamic microtubule tips via biased diffusion *Cell* **136** 865
[63] Emanuele M J, McCleland M L, Satinover D L and Stukenberg T P 2005 Measuring the stoichiometry and physical interactions between components elucidates the architecture of the vertebrate kinetochore *Mol. Biol. Cell* **16** 4882–93
[64] Kim Y, Heuser J E, Waterman C M and Cleveland D W 2008 CENP-E combines a slow, processive motor and a flexible coiled coil to produce an essential motile kinetochore tether *J. Cell Biol.* **181** 411–9
[65] Suzuki A, Badger B L, Haase J, Ohashi T, Erickson H P, Salmon E D and Bloom K 2016 How the kinetochore couples microtubule force and centromere stretch to move chromosome *Nat. Cell Biol.* **18** 382–92
[66] Shi X, Wang P, Chen H and Xie P 2021 Studies of conformational changes of tubulin induced by interaction with kinesin using atomistic molecular dynamics simulations *Int. J. Mol. Sci.* **22** 6709
[67] Shi X X, Guo S K, Wang P Y, Chen H and Xie P 2019 All-atom molecular dynamics simulations reveal how kinesin transits from one-head-bound to two-heads-bound state *Proteins Struct. Funct. Bioinf.* **88** 545–57
[68] Price D J and Brooks C R 2004 A modified TIP3P water potential for simulation with Ewald summation *J. Chem. Phys.* **121** 10096–103
[69] Hess B, Kutzner C, van der Spoel D and Lindahl E 2008 GROMACS 4: algorithms for highly efficient, load-balanced, and scalable molecular simulation *J. Chem. Theory Comput.* **4** 435–47
[70] Hornak V, Abel R, Okur A, Strockbine B, Roitberg A and Simmerling C 2006 Comparison of multiple Amber force fields and development of improved protein backbone parameters *Proteins* **65** 712
[71] Hess B, Bekker H, Berendsen H J C and Fraaije J G E M 1997 LINCS: A linear constraint solver for molecular simulations *J. Comput. Chem.* **18** 1463–72
[72] Essmann U, Perera L and Berkowitz M L 1995 A smooth particle mesh Ewald method *J. Chem. Phys.* **103** 8577
[73] Bussi G, Donadio D and Parrinello M 2007 Canonical sampling through velocity rescaling *J. Chem. Phys.* **126** 14101
[74] Berendsen H J C, Postma J P M, van Gunsteren W F, Di Nola A and Haak J R 1984 Molecular dynamics with coupling to an external bath *J. Chem. Phys.* **81** 3684–90
[75] Humphrey W, Dalke A and Schulten K 1996 VMD: visual molecular dynamics *J. Mol. Graph.* **14** 33–8